Chinese Journal of Structural Chemistry

REVIEW

Progress and Understanding on Catalysts with Well-defined Interface for Boosting CO_2 Conversion

Binran Zhao[1], Yiyi Zhao[1], Peng Liu[2], Yulong Men[2], Xinyu Meng[2] and Yunxiang Pan[2]*

[1]*School of Chemical Engineering, Northwest University, Xi'an 710069, China*

[2]*Department of Chemical Engineering, School of Chemistry and Chemical Engineering, Shanghai Jiao Tong University, Shanghai 200240, China*

ABSTRACT Catalytic conversion of CO_2 into valuable chemicals like CH_3OH is the most promising way to alleviate CO_2 emission for solving the serious climate change issue. Multi-component catalysts with well-defined interface show outstanding performance in CO_2 conversion due to the synergistic effects and multifunctional properties caused by the well-defined interface. A discharge technique, named as cold plasma, has been recognized as an excellent strategy for tuning catalyst interface properties. The temperature of cold plasma is lower than 200 ºC, and can be further lowered to room temperature by simply changing the operation conditions of cold plasma. The lower temperature of cold plasma can well maintain the catalyst structures, especially the porous structures. When conducting cold plasma, in addition to nontoxic working gases like Ar and air, no harmful substances are used. Cold-plasma-prepared catalysts have unique interface properties, and thereby exhibit superior performance in CO_2 conversion over the catalysts prepared by traditional methods. The present review summarizes the progress about the cold-plasma-prepared catalysts for CO_2 conversion, discusses the origin for the outstanding catalytic performance, and proposes the challenges and opportunities for further studies. This will stimulate more deep insights into the cold-plasma-prepared catalysts with well-defined interface properties for achieving more efficient CO_2 conversion.

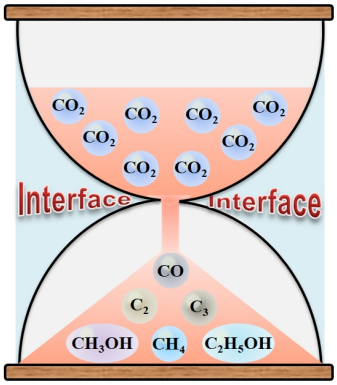

Keywords: carbon dioxide, heterogeneous catalysis, interface effect, noble metal, transition metal, cold plasma

n INTRODUCTION

Dramatically increasing emission of CO_2 into atmosphere is the most serious challenge faced by mankind.[1] Converting CO_2 into valuable chemicals like CH_3OH via thermocatalysis, photocatalysis and electrocatalysis processes is the most promising way to alleviate CO_2 emission.[1-3] Multi-component composite catalysts with well-defined interface have been widely explored for CO_2 conversion.[1-5] The interface among the catalyst components can efficiently trigger the synergistic effects of the catalyst components, formation of highly dispersed catalytic active sites and flexible transfer of the reaction intermediates to the catalytic active sites (Figure 1).[1-5] Besides, the interface has been shown to provide catalytic active sites for CO_2 adsorption and conversion.[6-8] This makes the activity, selectivity and stability of multi-component composite catalysts with well-defined interface much better than those obtained by using the catalyst components separately.[1-8] How to finely tune the catalyst interface has thereby been a hot topic. Common methods usually use calcination above 300 ºC, H_2-reduction at temperature higher than 300 ºC, hydrothermal process and solvothermal process.[9-17] Under high temperatures, the catalyst structures can be easily destroyed, especially for porous catalysts, *e.g.* zeolites and metal-organic frameworks.[15-17] Moreover, harmful substances, *e.g.* acid, alkali and organic reagent, are usually used in the common methods.[9-15] Therefore, methods operated under mild conditions at low temperature without using harmful substances are highly desired for fabricating more efficient catalysts to enhance CO_2 conversion.

A discharge technique, named as cold plasma, has been recognized as an excellent alternative to common methods for tuning the interface properties of multi-component catalysts for CO_2 conversion.[18-22] Cold plasma is formed by ionizing a gas or a gas mixture, *e.g.* Ar, air, O_2 and N_2, by applying a voltage of 100–200 V on the electrodes of cold plasma equipment (Figure 2). Dielectric barrier discharge, glow discharge and radio frequency discharge are typical cold plasma.[18-22] Cold plasma contains a large amount of electrons which have energies ranging from 5 to 10 eV and move fast as well as cations and anions.[18-22] However, the temperature of cold plasma is lower than 200 ºC, and can be further lowered to room temperature by simply changing the operation conditions.[18-22] Although lower than 200 ºC, the energy of the electrons in cold plasma is so high that collisions of the electrons with substances can efficiently trigger various reactions, *e.g.* dissociation of metal salts into metal oxides, reduction of metal cations into metallic atoms, formation of strong chemical bonds at the interface among catalyst components, creation of oxygen vacancies and functional groups on catalyst surfaces, and doping metal

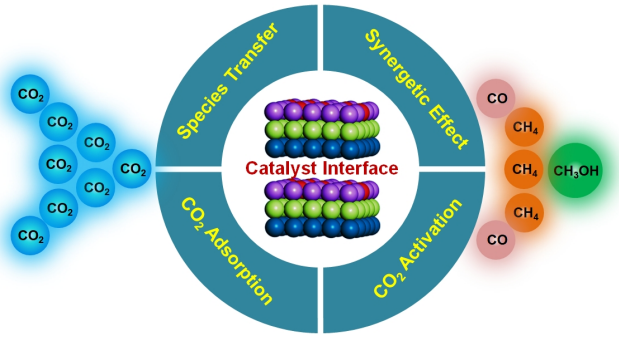

Figure 1. Schematic for the roles of catalyst interface in CO_2 conversion.

DOI: 10.14102/j.cnki.0254-5861.2022-0024

Chinese Journal of Structural Chemistry

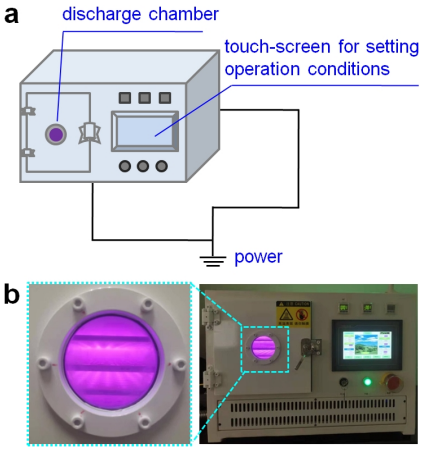

Figure 2. (a) Schematic for the set-up of cold plasma. (b) Image taking during the preparation process of catalysts by using cold plasma.

and non-metal atoms into catalysts.[18-27] The relatively low temperature of cold plasma can well maintain the structural properties of catalysts, especially the porous structures. In the cold plasma process, in addition to the nontoxic working gases like Ar, air, O_2 and N_2, no harmful acids, alkalis and organic reagents are used. Moreover, the interface properties of catalysts can be finely tuned by simply changing the operation conditions of cold plasma, *e.g.* working gas, power, time and pressure.[18-27]

The cold-plasma-prepared catalysts have unique interface properties, and thereby exhibit superior performances in CO_2 conversion over the catalysts prepared by using the traditional methods.[18-32] In order to further extend the application of outstanding catalysts prepared by using cold plasma, a critical review on the progress in the area is highly desired. There have been many reviews on CO_2 conversion, but these reviews paid very little attention to the cold-plasma-prepared catalysts. Herein, we discuss the progresses on the cold-plasma-prepared catalysts with well-defined interface for CO_2 conversion, demonstrate the origins of the excellent catalytic performance and the reaction mechanisms, and propose the challenges and opportunities for further studies.

n SUPPORTED NOBLE METAL CATALYSTS

Supported noble metal catalysts, formed by loading noble metal nanoparticles (*e.g.* Pt, Pd and Ir nanoparticles) on supports (*e.g.* metal oxides, zeolites and metal-organic frameworks), are the most widely explored catalysts for CO_2 conversion.[33-35] The properties of the metal-support interface determine the features of noble metal nanoparticles, *e.g.* size, morphology, defects and crystal planes, and thus influence the features of catalytic active sites, *e.g.* amount, distribution and structure.[33-35] Efficiently controlling the properties of the metal-support interface is crucial for improving the performance of the supported noble metal catalysts in CO_2 conversion. Traditional methods for preparing the supported noble metal catalysts mainly include two steps: (i) loading noble metal cations on supports, and (ii) reducing the noble metal cations by H_2 at temperature higher than 300 ºC.[33-38] The reduction step by using H_2 converts noble metal cations into noble metal atoms at zero valence state, and drives the transfer and combination of noble metal atoms to form noble metal nanoparticles, thus leading to the supported noble metal catalysts. But, the catalysts prepared by traditional methods show relatively weak metal-support interaction, thus suffering from serious aggregation of noble metal nanoparticles. Moreover, the high temperature of the H_2-reduction step further promotes the aggregation of noble metal nanoparticles. Therefore, on the catalysts prepared by traditional methods, the noble metal nanoparticles easily aggregate into larger sizes, and thereby show mixed crystal structures, with crystal planes having lower catalytic activity and more defects.[33-35] This inevitably decreases the activity, selectivity and stability of catalysts in CO_2 conversion.

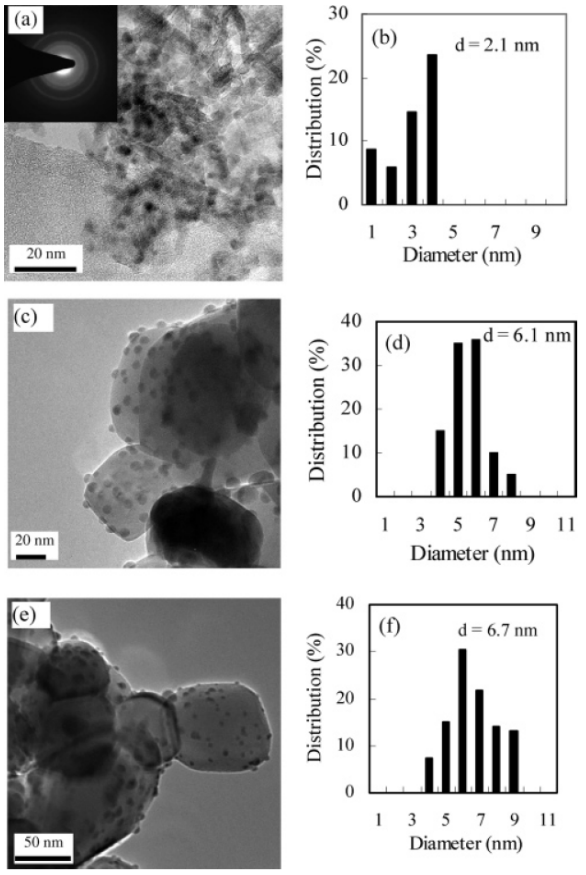

Figure 3. TEM images and size distributions of catalysts prepared by the cold-plasma-driven reduction: (a and b) Pd/Al_2O_3, (c and d) Ag/TiO_2, (e and f) Au/TiO_2. Reproduced with permission from Ref.[39]

A cold-plasma-driven room-temperature H_2-free reduction was developed for reducing noble metal cations into metallic states in the absence of H_2 at temperature lower than 30 ºC.[39-47] In the cold-plasma-driven reduction, only Ar is used as the working gas of cold plasma. Collisions of the high-energy electrons of cold plasma with noble metal species (cations, atoms, clusters, nanoparticles) and supports lead to three aspects: (i) reducing noble metal cations into metallic states, (ii) promoting the transfer and combination of noble metal atoms to form nanoparticles, and (iii) creating bond interactions at metal-support interface. The low temperature of cold-plasma-driven reduction as well as the bond

DOI: 10.14102/j.cnki.0254-5861.2022-0024

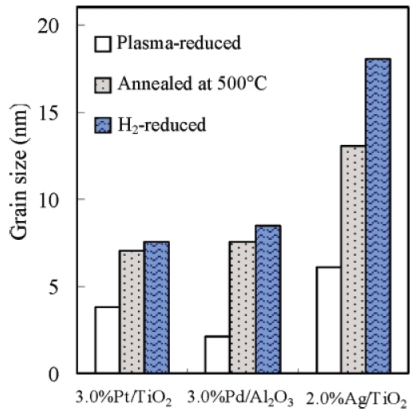

Figure 4. Particle size of catalysts prepared by different methods. Reproduced with permission from Ref.[39]

interactions formed at metal-support interface efficiently suppress the aggregation of noble metal nanoparticles, and create well-defined metal-support interface (Figure 3).[39-47] This results in highly dispersed noble metal nanoparticles which have more perfect crystal structure, more uniform morphology, smaller size and more perfect crystal planes with higher catalytic activity, as compared with the catalysts prepared by traditional H_2-reduction (Figures 3 and 4).[39-47] For example, the sizes of noble metal nanoparticles on Pt/TiO_2, Pd/Al_2O_3 and Ag/TiO_2 prepared by the cold-plasma-driven reduction are about 4.0, 2.0 and 6.0 nm, respectively, smaller than those on the catalysts prepared by the traditional H_2-reduction (about 7.0, 8.0 and 18.0 nm, respectively) (Figure 4).[39] Moreover, the properties of metal-support interface and noble metal nanoparticles can be finely tuned by simply changing the operation conditions of the cold-plasma-driven reduction *e.g.* time, pressure, power and content of the metal cations. For example, the size of Au nanoparticles increased from 3.2 to 19.4 nm by tuning the content of the Au cations during the cold-plasma-driven reduction (Figure 5).[40] Apart from the formation of well-defined metal-support interface, some oxygen atoms from the supports may move to the metal nanoparticles, thus producing an ultrathin oxide shell on the metal nanoparticles.[18-27] This can also help to suppress the aggregation of metal nanoparticles. With the cold-plasma-driven reduction, many efficient supported noble metal catalysts with well-defined metal-support interface have been fabricated, *e.g.* supported Au, Pt, Pd, Rh, Ir and Ag catalysts.[39-47]

Zhao *et al.* applied the cold-plasma-driven reduction to prepare an Al_2O_3-supported Ir catalyst (Ir/Al_2O_3-P), and compared the structural properties and catalytic performance of Ir/Al_2O_3-P in producing syngas (CO + H_2) from CO_2-reforming of CH_4 with those of the catalyst prepared by the traditional H_2-reduction at 600 ºC for 3 h (Ir/Al_2O_3-H).[41] In CO_2-reforming of CH_4 at 750 ºC, Ir/Al_2O_3-P showed a CO_2 conversion of 73% and a CH_4 conversion of 67%, which were about twice higher than those on Ir/Al_2O_3-H (CO_2: 36%, CH_4: 33%).[41] The enhanced catalytic performance could be due to the well-defined Ir-Al_2O_3 interface on Ir/Al_2O_3-P. The well-defined Ir-Al_2O_3 interface suppressed the aggregation of Ir nanoparticles, thus leading to a higher Ir nanoparticle dispersion (83.95%), a smaller average Ir nanoparticle size (1.18 nm) and a larger active surface area (2.268 $m^2 \cdot g^{-1}$) on Ir/Al_2O_3-P, as compared with those on Ir/Al_2O_3-H (30.09%, 3.29 nm, 0.813 $m^2 \cdot g^{-1}$).[41] This resulted in abundant active Ir sites for dissociating CH_4 into CH_x species and H_2. The well-defined Ir-Al_2O_3 interface provided abundant active sites for the adsorption and activation of CO_2 to form more CO_2^{d-} species.[48,49] The well-defined Ir-Al_2O_3 interface facilitated the transfer of CH_x species from Ir nanoparticles to the CO_2^{d-} adsorbed at Ir-Al_2O_3 interface, and drove the reaction of CO_2^{d-} with CH_x to form CO and H_2. The multiple roles of the well-defined Ir-Al_2O_3 interface could be the origin for the enhanced performance of Ir/Al_2O_3-P in CO_2-reforming of CH_4.

By using cold plasma, Rui *et al*. fabricated a Pd-P/In_2O_3 catalyst.[42] In CO_2 hydrogenation with H_2, the cold-plasma-prepared Pd-P/In_2O_3 showed a CO_2 conversion > 20%, a CH_3OH selectivity > 70% and a space-time yield (STY) of CH_3OH up to 0.89 $g_{MeOH}\ h^{-1} \cdot g_{cat}^{-1}$, which are higher than those on Pd/In_2O_3 prepared by traditional method.[42] The well-defined Pd-In_2O_3 interface could be responsible for the better catalytic performance of Pd-P/In_2O_3. Due to the well-defined Pd-In_2O_3 interface, the Pd nanoparticles on Pd-P/In_2O_3 had an average size as small as 3.6 nm, and mainly exposed the Pd(111) plane which provided the catalytic active sites for H_2 dissociation.[42] This led to more catalytic active Pd sites for H_2 dissociation, thus producing abundant H atoms on Pd nanoparticles. The well-defined Pd-In_2O_3 interface facilitated the transfer of the H atoms from Pd nanoparticles to In_2O_3, and the reaction of H atoms with the O atoms of In_2O_3 created an

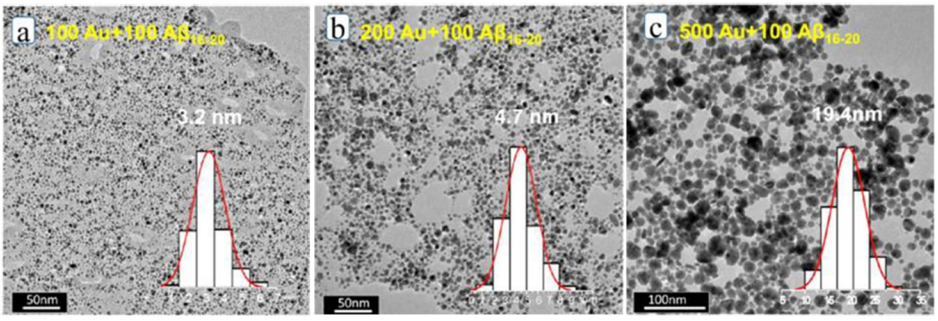

Figure 5. TEM images and sizes of supported Au nanoparticles prepared under different cold plasma conditions: (a) 100 μM $HAuCl_4$ with 100 μM $A\beta_{16-20}$ aqueous solutions (100Au + 100$A\beta_{16-20}$), (b) 200Au + 100$A\beta_{16-20}$, (c) 500Au + 100$A\beta_{16-20}$. Reproduced with permission from Ref.[40]

DOI: 10.14102/j.cnki.0254-5861.2022-0024

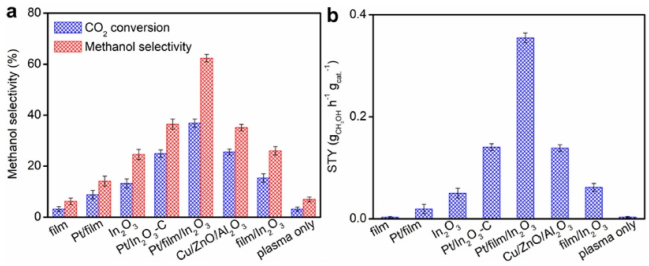

Figure 6. (a) CO_2 conversion efficiency and CH_3OH selectivity as well as (b) STY of CH_3OH on different catalysts. Reproduced with permission from Ref.[43]

appropriate amount of oxygen vacancies at the Pd-In_2O_3 interface.[42] A monodentate formate (HCOO) species was demonstrated to be a key intermediate for CH_3OH production from the CO_2 hydrogenation on Pd-P/In_2O_3.[42] The oxygen vacancies at the Pd-In_2O_3 interface promoted CO_2 adsorption, activation and hydrogenation to form the key HCOO intermediate for CH_3OH production, and stabilized HCOO for further hydrogenation.[42] This favored for the CH_3OH production from CO_2 hydrogenation on Pd-P/In_2O_3. The reverse water gas shift (RWGS) reaction was the main competitive reaction for CH_3OH formation during CO_2 hydrogenation.[42] The synergistic effects between Pd nanoparticles and In_2O_3 due to the well-defined Pd-In_2O_3 interface helped to suppress the RWGS reaction through limiting the formation of COOH groups on catalyst.[42] This was also benefit for producing CH_3OH from CO_2 hydrogenation on Pd-P/In_2O_3. Moreover, the more abundant H atoms formed on Pd nanoparticles as well as the flexible transfer of the H atoms from Pd nanoparticles to the CO_2 adsorbed at the Pd-In_2O_3 interface efficiently lowered the activation barriers for CH_3OH formation through the HCOO reaction route.[42] This further enhanced the CH_3OH formation from CO_2 hydrogenation on Pd-P/In_2O_3.

Men *et al.* reported a Pt/film/In_2O_3 catalyst prepared by using the cold-plasma-driven reduction.[43] During CO_2 hydrogenation on Pt/film/In_2O_3, a CO_2 conversion of 37.0%, a CH_3OH selectivity of 62.6% and a STY of CH_3OH up to 0.355 $g_{MeOH}\cdot h^{-1}\cdot g_{cat.}^{-1}$ were achieved (Figure 6).[43] These were much better than those on Pt/In_2O_3-C prepared by the traditional H_2-reduction method and commercial CuZnAl catalyst (Figure 6).[43] Due to the well-defined Pt-In_2O_3 interface, the Pt nanoparticles on Pt/film/In_2O_3 had a more perfect crystal structure, a higher dispersion and a smaller average size (3.5 nm), and exposed more Pt(111) plane which was more catalytic active to H_2 adsorption and dissociation.[43] Different from Pt/film/In_2O_3, a serious aggregation of Pt nanoparticles was observed on Pt/In_2O_3-C, resulting in the average Pt nanoparticle size on Pt/In_2O_3-C as large as 10.2 nm.[43] Thereby, as compared with Pt/In_2O_3-C, there are more active Pt sites on Pt/film/In_2O_3 for dissociating H_2 to form abundant H atoms. The well-defined Pt-In_2O_3 interface created more active sites for improving the adsorption and activation of CO_2 on Pt/film/In_2O_3. In addition, as compared with those on Pt/In_2O_3-C, the transfer of H atoms from Pt nanoparticles to the CO_2 adsorbed at Pt-In_2O_3 interface was more flexible due to the well-defined Pt-In_2O_3 interface on Pt/film/In_2O_3. The more abundant H atoms, improved CO_2 adsorption and activation as well as the flexible transfer of H atoms promoted the formation of methoxy species (CH_3O) which was a key species in producing CH_3OH from CO_2 hydrogenation, thus enhancing the CH_3OH production from CO_2 hydrogenation on Pt/film/In_2O_3.

n SUPPORTED TRANSITION METAL CATALYSTS

The supported noble metal catalysts have superior activity, selectivity and stability to CO_2 conversion. But the high price and scarce resource of noble metals limit the large-scale commercial applications of the supported noble metal catalysts. Supported transition metal catalysts, *e.g.* supported Ni, Co and Fe catalysts, which have low cost and abundant resource, are highly desired for CO_2 conversion.[50-55] However, the activity, selectivity and stability of supported transition metal catalysts are still lower, and need further improvement. Traditional methods to prepare supported transition metal catalysts mainly include three steps: (i) loading transition metal salts (*e.g.* nickel nitrate) on the supports through wet impregnation, (ii) conducting calcination above 300 ºC to decompose the transition metal salts into transition metal oxides, and (iii) reducing the transition metal oxides by H_2 at temperature higher than 300 ºC to form the supported transition metal catalysts.[50-55] Catalysts prepared by the traditional methods usually have weak metal-support interaction, and thereby suffer from transition metal nanoparticle aggregation.[50-55] The relatively high temperature of calcination and H_2-reduction further promote the aggregation of transition metal nanoparticles. Thus, on catalysts prepared by using the traditional methods, the transition metal nanoparticles generally show mixed crystal structures, with the crystal planes having low catalytic activity and more defects.[50-55] This was proposed to be the origin for lower efficiency of the supported transition metal catalysts in CO_2 conversion. Besides, for CO_2 conversion, *e.g.* CO_2-reforming of CH_4, carbon deposition occurs easily, due to CO disproportionation and splitting of carbon-containing species like CH_4.[50-55] The transition metal catalysts are poor in resisting to carbon deposition.[50-55] The deposited carbon atoms can incorporate into the lattice of transition metals to convert transition metals into transition metal carbides, and can insert

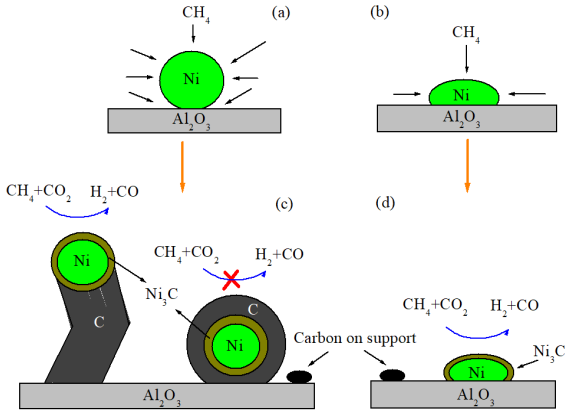

Figure 7. Carbon deposition on Ni/Al_2O_3 catalyst during CO_2-reforming of CH_4. Reproduced with permission from Ref.[58]

DOI: 10.14102/j.cnki.0254-5861.2022-0024

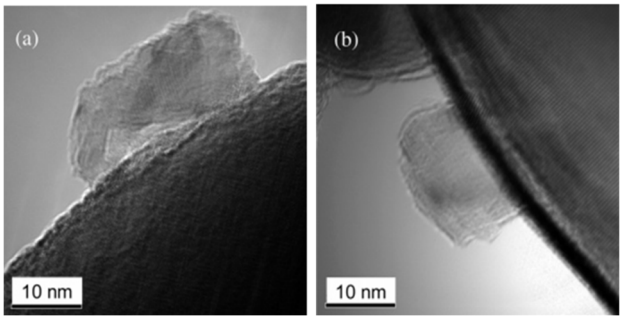

Figure 8. TEM images of (a) NiO/Ta_2O_5 and (b) NiO/ZrO_2 prepared by using the cold-plasma-assisted process. Reproduced with permission from Ref.[60]

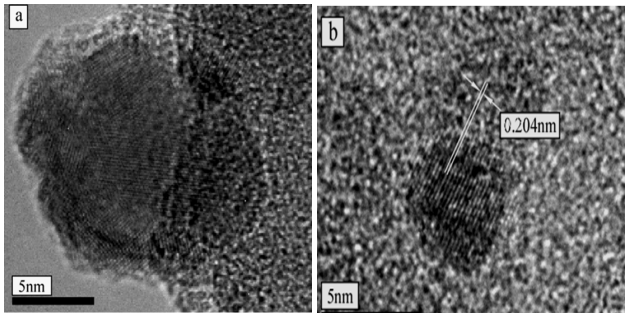

Figure 9. HRTEM images of Ni nanoparticles on (a) C-Ni/SiO_2 and (b) P-Ni/SiO_2. Reproduced with permission from Ref.[61]

into the metal-support interface to separate transition metal nanoparticles and supports (Figure 7).[56-59] The deposited carbon atoms can also accumulate around transition metal nanoparticles to wrap transition metal nanoparticles (Figure 7), thus hindering the adsorption and conversion of reactants on catalytic active sites.[56-59] The serious carbon deposition inevitably decreases the catalytic performance of the supported transition metal catalysts.

A cold-plasma-assisted process has been developed to prepare the supported transition metal catalysts with well-defined interface for achieving more efficient CO_2 conversion.[59-72] Different from supported noble metal catalysts, when using H_2-free cold plasma to prepare supported transition metal catalysts, the high-energy electrons of cold plasma cannot reduce transition metal cations into metallic states. The cold-plasma-assisted preparation of the supported transition metal catalysts mainly includes three steps: (i) loading transition metal salts on supports through wet impregnation, (ii) treating the (transition metal salts)-support sample by cold plasma to decompose transition metal salts into transition metal oxides, and (iii) reduction of transition metal oxides by H_2 at temperature higher than 300 ºC to form the supported transition metal catalysts. The second step with cold plasma plays two crucial roles. Firstly, collisions of the high-energy electrons of cold plasma with transition metal salts decompose transition metal salts into transition metal oxides. Secondly, collisions of the high-energy of electrons of cold plasma with transition metal oxide nanoparticles and supports create stronger bond interactions between transition metal oxide nanoparticles and supports, and tightly anchor transition metal oxide nanoparticles on supports (Figure 8).[60] Due to the stronger interactions between transition metal oxide nanoparticles and supports, the metal-support interface on the catalysts after H_2 reduction is still well-defined, although the reduction temperature is higher than 300 ºC. This makes the transition metal nanoparticles on the catalysts prepared through the cold-plasma-assisted process exhibit perfect crystal structure, uniform morphology, smaller size and more crystal planes with higher catalytic activity. Therefore, the performance of the supported transition metal catalysts prepared by the cold-plasma-assisted process in CO_2 conversion is better than those on the supported transition metal catalysts prepared by traditional methods, even better than those on the supported noble metal catalysts.

Pan *et al.* fabricated a SiO_2-supported Ni catalyst (P-Ni/SiO_2) via the cold-plasma-assisted process, and compared the performance of P-Ni/SiO_2 in CO_2-reforming of CH_4 with that of the C-Ni/SiO_2 catalyst prepared by traditional method without cold plasma.[61] At 600 ºC, P-Ni/SiO_2 showed CO_2 and CH_4 conversion of about 50% and 40%, respectively, which were higher than those on C-Ni/SiO_2 (CO_2: 40%, CH_4: 25%). More importantly, P-Ni/SiO_2 was much more efficient in suppressing carbon deposition than C-Ni/SiO_2. This could be caused by the well-defined Ni-SiO_2 interface on P-Ni/SiO_2. Due to the well-defined Ni-SiO_2 interface, the Ni nanoparticles on P-Ni/SiO_2 showed a higher dispersion (17.0%), a smaller average size (5.9 nm), a larger active surface area (9.1 $m^2 \cdot g^{-1}$) and more Ni(111) planes, as compared with those on C-Ni/SiO_2 (10.7%, 9.4 nm, 5.7 $m^2 \cdot g^{-1}$) (Figure 9).[61] Decomposition of CH_4 ($CH_4 \rightarrow C + H_2$) on Ni nanoparticle produced carbon atoms which were the source of carbon deposition.[61] The carbon atoms can react with CO_2 to form CO ($CO_2 + C \rightarrow 2CO$).[61] This was the way to eliminate carbon from catalyst. The carbon formation-elimination balance determined the amount of the carbon deposited on catalyst, and was closely related to the rates of ($CH_4 \rightarrow C + H_2$) and ($CO_2 + C \rightarrow 2CO$) reactions. If the ($CO_2 + C \rightarrow 2CO$) reaction proceeded more slowly than the ($CH_4 \rightarrow C + H_2$) reaction, the carbon atoms precipitated and polymerized. The ($CH_4 \rightarrow C + H_2$) reaction was sensitive to the structural properties of Ni nanoparticles. The Ni nanoparticles with more Ni(111) planes exposed are shown to be more efficient to suppress carbon formation from the ($CH_4 \rightarrow C + H_2$) reaction, as compared with the Ni nanoparticles with more distortions and defects.[61] Due to the lower crystallinity and more defects of Ni nanoparticles on C-Ni/SiO_2, the carbon formation and precipitation proceeded readily. Moreover, due to weak Ni-SiO_2 interaction, the carbon atoms easily entered into the Ni-SiO_2 interface on C-Ni/SiO_2. This resulted in the serious carbon deposition on C-Ni/SiO_2. Different from C-Ni/SiO_2, the Ni nanoparticles on P-Ni/SiO_2 had a more perfect crystallinity, less defects and more Ni(111) planes, thus suppressing the carbon formation from ($CH_4 \rightarrow C + H_2$) reaction. Thereby, the carbon formation rate on P-Ni/SiO_2 could be much lower than that on C-Ni/SiO_2. In addition, the well-defined Ni-SiO_2 interface created more abundant active sites for CO_2 adsorption and activation to form more $CO_2^{\delta-}$ species.[48] $CO_2^{\delta-}$ had a higher activity to react with the carbon atoms formed from the ($CH_4 \rightarrow C$

DOI: 10.14102/j.cnki.0254-5861.2022-0024

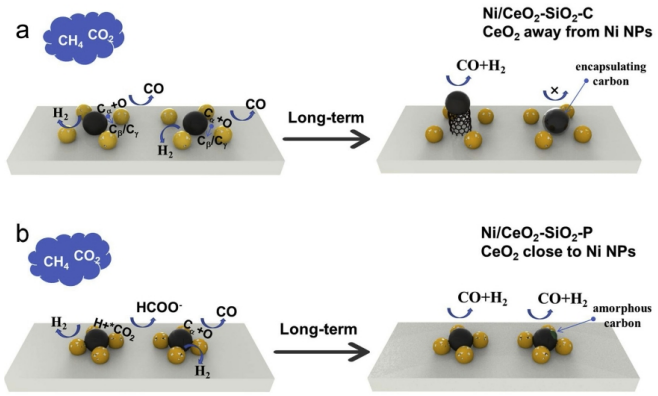

Figure 10. Proposed reaction pathways for the CO_2-reforming of CH_4 on (a) Ni/CeO_2-SiO_2-C and (b) Ni/CeO_2-SiO_2-P catalysts. Reproduced with permission from Ref.[62]

+ H_2) reaction, enhancing carbon elimination on P-Ni/SiO_2.[48] Thus, P-Ni/SiO_2 could have a higher carbon elimination rate than C-Ni/SiO_2. The lower carbon formation rate but higher carbon elimination rate are responsible for the greatly enhanced ability of P-Ni/SiO_2 in suppressing carbon deposition.

By using the cold-plasma-assisted preparation process, Yan *et al.* added CeO_2 into Ni/SiO_2 to form a Ni/CeO_2-SiO_2-P catalyst for CO_2-reforming of CH_4.[62] On the catalyst prepared by the traditional method without cold plasma (Ni/CeO_2-SiO_2-C), the Ni and CeO_2 nanoparticles were separately dispersed on SiO_2 to form Ni-SiO_2 and CeO_2-SiO_2 interfaces, but there was no Ni-CeO_2 interface (Figure 10).[62] On Ni/CeO_2-SiO_2-P, the CeO_2 nanoparticles located at the Ni-SiO_2 interface, and tightly interacted with both Ni nanoparticle and SiO_2 support (Figure 10).[62] The intimate Ni-CeO_2-SiO_2 interface on Ni/CeO_2-SiO_2-P played crucial roles in CO_2-reforming of CH_4. Firstly, the intimate Ni-CeO_2-SiO_2 interface provided more abundant active sites for CO_2 adsorption and activation to form more CO^{d-} species.[62] This promoted the reaction of CO_2^{d-} with the carbon atoms formed from the ($CH_4 \rightarrow C + H_2$) reaction, thus increasing the carbon elimination rate on Ni/CeO_2-SiO_2-P. Secondly, the intimate Ni-CeO_2-SiO_2 interface anchored the Ni nanoparticles on support firmly, and suppressed the aggregation of Ni nanoparticles.[62] This made the Ni nanoparticles on Ni/CeO_2-SiO_2-P have more perfect crystallinity which can efficiently suppress the carbon formation from the ($CH_4 \rightarrow C + H_2$) reaction. Therefore, the intimate Ni-CeO_2-SiO_2 interface suppressed carbon formation but promoted carbon elimination. This led Ni/CeO_2-SiO_2-P to have a higher ability in resisting to carbon deposition and a significantly improved stability in a long-term reaction (50 h).[62] Different from Ni/CeO_2-SiO_2-P, the catalytic performance of Ni/CeO_2-SiO_2-C decreased dramatically when conducting the CO_2-reforming of CH_4 for only 10 h, due to serious carbon deposition.[62] In-situ DRIFTs analyses were preformed to compare the mechanism of the CO_2-reforming of CH_4 on Ni/CeO_2-SiO_2-P with that on Ni/CeO_2-SiO_2-C.[62] On the DRIFTs spectra of Ni/CeO_2-SiO_2-C, bands attributed to CH_4, CO, carbonate species (CO_3^{2-}) and CO_2^{d-} were observed.[62] On the DRIFTs spectra of Ni/CeO_2-SiO_2-P, besides CH_4, CO, CO_3^{2-} and CO_2^{d-}, formate (HCOO) was also present,[62] indicating it could be formed as an important intermediate during the CO_2-reforming of CH_4 on Ni/CeO_2-SiO_2-P.[62] The formation of formate on Ni/CeO_2-SiO_2-P could be from the intimate Ni-CeO_2-SiO_2 interface. It has been revealed that the formation of (CO + H_2) from the CO_2-reforming of CH_4 *via* the reaction with formate as an intermediate proceeded more easily, both thermodynamically and kinetically.[62] Thereafter, the intimate Ni-CeO_2-SiO_2 interface promoted the formation of formate to enhance the (CO + H_2) production in CO_2-reforming of CH_4 on Ni/CeO_2-SiO_2-P.

Jia *et al.* reported a Ni/ZrO_2-P catalyst prepared by using the cold-plasma-assisted process for CO_2 methanation.[63] On the catalyst fabricated through the traditional high-temperature calcination (Ni/ZrO_2-C), Ni nanoparticles agglomerated on ZrO_2 and the Ni lattice were difficult to distinguish due to the highly disordered crystal structure (Figure 11).[63] On Ni/ZrO_2-P, Ni nanoparticles with an average size of about 10 nm were highly dispersed on ZrO_2, more Ni(111) planes with a higher catalytic activity were exposed, and well-defined Ni-ZrO_2 interface can be clearly seen

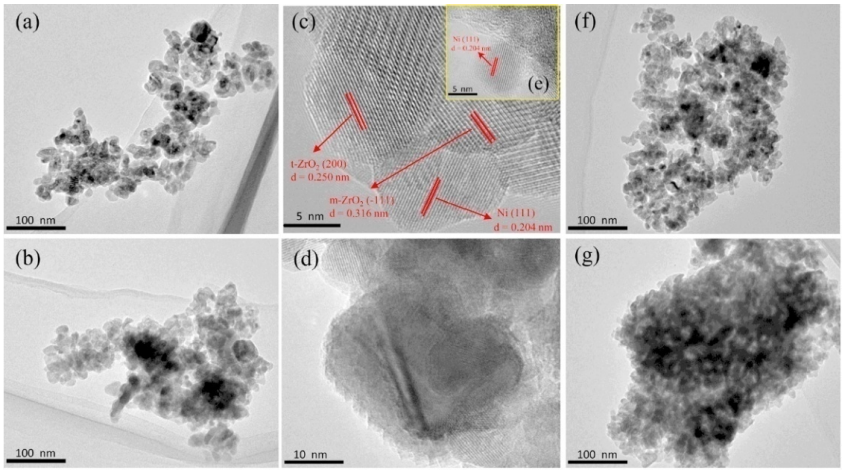

Figure 11. TEM images of (a) Ni/ZrO_2-P and (b) Ni/ZrO_2-C. HRTEM images of (c and e) Ni/ZrO_2-P and (d) Ni/ZrO_2-C. TEM images of (f) used Ni/ZrO_2-P after CO_2 methanation and (g) Ni/ZrO_2-C after CO_2 methanation. Reproduced with permission from Ref.[63]

DOI: 10.14102/j.cnki.0254-5861.2022-0024

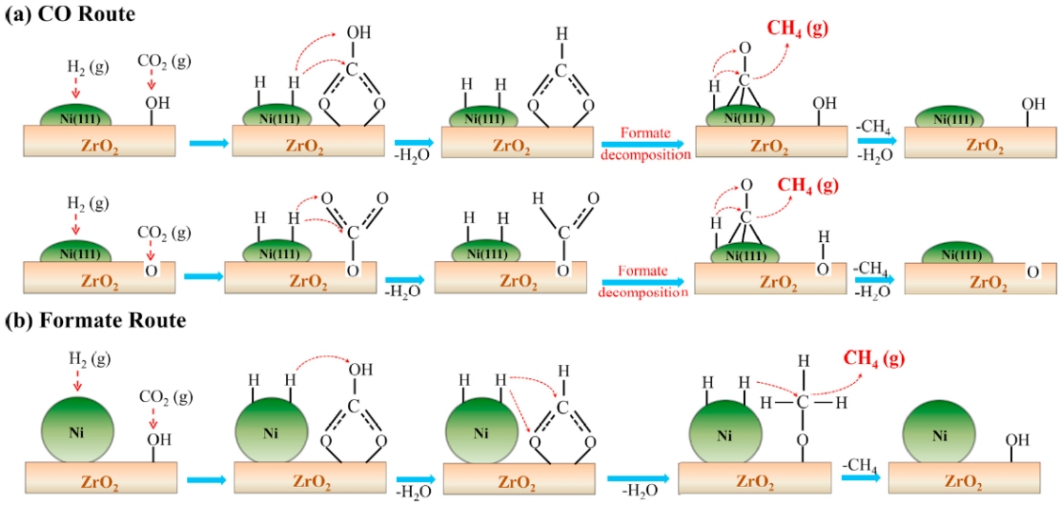

Figure 12. Proposed possible pathways for the CO_2 methanation reaction on (a) Ni/ZrO_2-P and (b) Ni/ZrO_2-C catalysts. Reproduced with permission from Ref. [63]

(Figure 11).[63] The well-defined Ni-ZrO_2 interface on Ni/ZrO_2-P suppressed the aggregation of Ni nanoparticles during the CO_2 methanation process, but serious aggregation of Ni nanoparticles occurred during the CO_2 methanation process on Ni/ZrO_2-C due to the weak Ni-ZrO_2 interaction (Figure 11).[63] The well-defined Ni-ZrO_2 interface on Ni/ZrO_2-P created oxygen vacancies which provided catalytic active sites for CO_2 adsorption and activation.[63] The conversion pathway of CO_2 methanation on Ni/ZrO_2-P was proposed as follows (Figure 12).[63] Adsorption and activation of CO_2 on the oxygen vacancies at Ni-ZrO_2 interface resulted in a $CO_3^{\delta-}$ species.[63] The Ni(111) planes promoted the H_2 dissociation to form abundant H atoms. The H atoms can be easily transferred to the Ni-ZrO_2 interface and reacted with $CO_3^{\delta-}$ to form a $HCOO^{\delta-}$ species which was subsequently decomposed into CO.[63] The formed CO migrated to the Ni(111) planes and reacted with H atoms to form CH_4 (Figure 12). The weak Ni-ZrO_2 interaction made the amount of oxygen vacancies on Ni/ZrO_2-C less than that on Ni/ZrO_2-P. This led the adsorption of CO_2 on Ni/ZrO_2-C to be very weak, and decreased the activation degree of the adsorbed CO_2, thus limiting the reaction of the adsorbed CO_2 with H atoms. In addition, different from Ni/ZrO_2-P, on Ni/ZrO_2-C, due to the lack of Ni(111) plane, the dissociation of H_2 into H atoms proceeded more difficultly. This further suppressed the hydrogenation of adsorbed CO_2. These aspects led the catalytic performance of Ni/ZrO_2-P in CO_2 methanation to be much better than that of Ni/ZrO_2-C. At 250 and 275 ºC, the CO_2 conversion on Ni/ZrO_2-P is 15.4% and 50.2%, respectively, which are much higher than those on Ni/ZrO_2-C (6.1% and 15.2%).[63]

By using cold plasma, Rui *et al.* fabricated a Ni/CeO_2-P catalyst for CO_2 methanation.[64] As compared with the Ni/CeO_2-C catalyst prepared by traditional method, Ni/CeO_2-P showed a much higher low-temperature activity to CO_2 methanation. At 275 ºC, the CO_2 conversion on Ni/CeO_2-P catalyst was 82.4%, whereas that on Ni/CeO_2-C was only 34.7%.[64] The CH_4 generation rate and selectivity on Ni/CeO_2-P were 100.3 $\mu mol \cdot g_{cat}^{-1} \cdot s^{-1}$ and 99.5%, respectively.[64] These were better than those on Ni/CeO_2-C. At the same CO_2 conversion efficiency, the reaction temperature on Ni/CeO_2-P was lower by 75 ºC than that on Ni/CeO_2-C.[64] The enhanced catalytic performance of Ni/CeO_2-P could be due to the well-defined Ni-CeO_2 interface. The well-defined Ni-CeO_2 interface provided more active sites for CO_2 adsorption and activation.[64] The well-defined Ni-CeO_2 interface made the size of Ni nanoparticles on Ni/CeO_2-P smaller than that on Ni/CeO_2-C, and thus created abundant active sites for H_2 dissociation to form more H atoms.[64] The well-defined Ni-CeO_2 interface facilitated the transfer of H atoms from Ni nanoparticles to CO_2 adsorbed at Ni-CeO_2 interface, thus promoting the reaction of the H atoms with the CO_2 adsorbed at the Ni-CeO_2 interface. It was the multiple roles of Ni-CeO_2 interface that resulted in the enhanced CH_4 production from the hydrogenation of CO_2 on Ni/CeO_2-P.[64]

Apart from Ni-based catalysts, cold plasma was also efficient for preparing many other supported transition metal catalysts, *e.g.* supported Co and Fe catalysts, as well as other types of noble-metal-free catalysts for CO_2 conversion.[56,65-72] For instance, Zheng *et al.* formed an In_2S_3-NiS modified MoO_3@MoS_2 catalyst (INS/MoO_3@MoS_2) by using cold plasma.[65] Different from the catalysts prepared through the traditional method in the absence of cold plasma, tight interface among In_2S_3, NiS, MoS_2 and MoO_3 were formed on INS/MoO_3@MoS_2.[65] The rigorous In_2S_3-NiS-MoS_2-MoO_3 interface created well-defined interfacial heterojunctions, and thus promoted the CH_4 production from the photocatalytic reduction of CO_2, with the CH_4 product rate as high as 49.11 $\mu mol \cdot g^{-1} \cdot h^{-1}$.[65] Due to the formation of the rigorous In_2S_3-NiS-MoS_2-MoO_3 interface, some additional states were created between the conduction band and the valence band of the catalyst.[65] This helped to extend the wavelength range of the light absorbed by catalyst.[65] The rigorous In_2S_3-NiS-MoS_2-MoO_3 interface also favored for the separation and transfer of the photogenerated charge carriers, thus promoting more photogenerated electrons for surface reactions.[65] Besides, due to the tight In_2S_3-NiS-MoS_2-MoO_3 interface, more catalytic active sites were formed for the adsorption and conversion of reactants, thus resulting in more activated reactants for surface reactions.[65] The improved light absorption, promoted charge separation and more catalytic active

DOI: 10.14102/j.cnki.0254-5861.2022-0024

sites for reactant adsorption and conversion enhanced the production of CH_4 from the photocatalytic reduction of CO_2 on INS/MoO_3@MoS_2.

n CONCLUSIONS AND PERSPECTIVE

In summary, the interface on multi-component catalysts triggers valuable synergistic effects and multifunctional properties, flexible transfer of active species and reaction intermediates, and highly dispersed catalytic active sites (*e.g.* noble metal and transition metal nanoparticles), thus playing crucial roles in enhancing the CO_2 conversion efficiency. Cold plasma has been demonstrated to be an excellent and simple strategy to finely tune catalyst interface properties for improving CO_2 conversion efficiency. The most attractive point of the cold plasma process is that the energy of the electrons in cold plasma is as high as 5–10 eV but the operation temperature of cold plasma is lower than 200 ºC. By simply changing the conditions of cold plasma, *e.g.* time, power and pressure, the operation temperature of cold plasma can be lowered to room temperature. Thus, when conducting cold plasma for preparing catalysts, the catalyst interface properties can be efficiently tuned. At the same time, the structural features of catalysts can be well maintained, *e.g.* the porous structures. The cold-plasma-prepared catalysts exhibit superior performance in CO_2 conversion over the catalysts prepared by the traditional methods, due to their unique interface properties. However, there are still several issues on cold-plasma-prepared catalysts required to be further studied detailedly.

Firstly, better understanding on the exact roles of the catalyst interface in CO_2 conversion is necessary. There have been a large amount of studies focusing on the influence of catalyst interface on CO_2 conversion, including both experiments and theoretical calculations. The interface sites were revealed to be the active sites for CO_2 adsorption and activation. However, the exact site for the conversion of adsorbed CO_2 is still unclear. Some studies proposed that other reactants transfer to the interface sites and react with the adsorbed CO_2, while some studies reported that the adsorbed CO_2 was firstly activated into intermediates like formate and CO at the interface sites, and then the intermediates migrated to the sites on the supported metal nanoparticles and react with other reactants. More detailed studies have to be conducted, especially experiments like in-situ FTIR and theoretical calculations. But, due to the high complexity of the reaction, the construction of an ideal model matching well with the real system is still a challenge. In addition, during the reaction process, the interface properties could change, due to the interaction of CO_2 with the interface sites. More studies have to be done for clarifying the changes of the interface properties during the reaction process.

Secondly, better understanding on the exact mechanism of the change in interface properties during the cold plasma process is necessary. Collisions of the high-energy electrons in cold plasma with the catalyst components were proposed to be the main drive to create stronger interactions among the catalyst components, thus fabricating the well-defined interface properties. However, in addition to the electrons, a large number of other species, *e.g.* atoms, anions, radicals and cations, also exist in cold plasma. The roles of different species produced from cold plasma in tuning the catalyst interface properties have to be more detailedly studied, by using both experimental and theoretical observations. However, because cold plasma is a very complex system, studies on it need knowledge not only from chemistry and material but also from many other areas like physics, engineering and machine.

Due to the outstanding performance of cold-plasma-prepared catalysts in CO_2 conversion, finely tuning the interface properties by using cold plasma has stimulated numerous studies. We believe that, due to the continued efforts on optimizing the equipments and operation conditions of cold plasma as well as the worldwide attention on CO_2 utilization, massive application of the cold-plasma-prepared catalysts in industry will come true in the near future.

n ACKNOWLEDGEMENTS

This work is supported by the National Natural Science Foundation of China (No. 21922807 and 22078193), Double Thousand Plan of Jiangxi Province (461654, jxsq2019102052) and Shaanxi Provincial Key Research and Development Program (No. 2020ZDLGY11-06).

n AUTHOR INFORMATION

Corresponding author. Email: yxpan81@sjtu.edu.cn (Yunxiang Pan).

n COMPETING INTERESTS

The authors declare that they have no competing interests.

n ADDITIONAL INFORMATION

Full paper can be accessed via
http://manu30.magtech.com.cn/jghx/EN/10.14102/j.cnki.0254-5861.2022-0024
For submission: https://mc03.manuscriptcentral.com/cjsc

n REFERENCES

(1) Melchionna, M.; Fornasiero, P.; Prato, M.; Bonchio, M. Electrocatalytic CO_2 reduction: role of the cross-talk at nano-carbon interfaces. *Energy Environ. Sci.* **2021**, 14, 5816–5833.

(2) Kattel, S.; Liu, P.; Chen, J. G. Tuning selectivity of CO_2 hydrogenation reactions at the metal/oxide interface. *J. Am. Chem. Soc.* **2017**, 139, 9739–9754.

(3) Ma, W.; He, X.; Wang, W.; Xie, S.; Zhang, Q.; Wang, Y. Electrocatalytic reduction of CO_2 and CO to multi-carbon compounds over Cu-based catalysts. *Chem. Soc. Rev.* **2021**, 50, 12897–12914.

(4) Chen, J.; Wang, L. Effects of the catalyst dynamic changes and influence of the reaction environment on the performance of electrochemical CO_2 reduction. *Adv. Mater.* **2021**, 2103900.

(5) Liu, G.; Wong, W. S. Y.; Kraft, M.; Ager, J. W.; Vollmer, D.; Xu, R. Wetting-regulated gas-involving (photo) electrocatalysis: biomimetics in energy conversion. *Chem. Soc. Rev.* **2021**, 50, 10674–10699.

(6) Meng, X. Y.; Peng, C.; Jia, J.; Liu, P.; Men, Y. L.; Pan, Y. X. Recent progress and understanding on In_2O_3-based composite catalysts for boosting CO_2 hydrogenation. *J. CO_2 Util.* **2022**, 55, 101844.

(7) Xie, B.; Lovell, E.; Tan, T. H.; Jantarang, S.; Yu, M.; Scott, J.; Amal, R. Emerging material engineering strategies for amplifying photothermal het-

erogeneous CO_2 catalysis. *J. Energy Chem.* **2021**, 59, 108–125.
(8) Lu, H.; Tournet, J.; Dastafkan, K.; Liu, Y.; Ng, Y. H.; Karuturi, S. K.; Zhao, C.; Yin, Z. Noble-metal-free multicomponent nanointegration for sustainbale energy conversion. *Chem. Rev.* **2021**, 121, 10271–10366.
(9) Nam, D. H.; Luna, P. D.; Rosas-Hernández, A.; Thevenon, A.; Li, F.; Agapie, T.; Peters, J. C.; Shekhah, O.; Eddaoudi, M.; Sargent, E. H. Molecular enhancement of heterogeneous CO_2 reduction. *Nat. Mater.* **2020**, 19, 266–276.
(10) Mehla, S.; Kandjani, A. E.; Babarao, R.; Lee, A. F.; Periasamy, S.; Wilson, K.; Ramakrishna, S.; Bhargava, S. K. Porous crystalline framworks for thermocatalytic CO_2 reduction: an emerging paradigm. *Energy Environ. Sci.* **2021**, 14, 320–352.
(11) Pan, Y. X.; Wang, Z. J.; Cheng, D. G.; Wang Z. Hydrogenation of CO_2 in the absence of noble metals. *Greenhouse Gas. Sci. Technol.* **2021**, 11, 1169–1170.
(12) De, S.; Dokania, A.; Ramirez, A.; Gascon, J. Advances in the design of heterogeneous catalysts and thermocatalytic processes for CO_2 utilization. *ACS Catal.* **2020**, 10, 14147–14185.
(13) Wang, Z. J.; Song, H.; Liu, H.; Ye, J. Coupling of solar energy and thermal energy for carbon dioxide reduction: status and prospects. *Angew. Chem. Int. Ed.* **2020**, 59, 8016–8035.
(14) Ghoussoub, M.; Xia, M.; Duchesne P. N.; Segal, D.; Ozin, G. Principles of photothermal gas-phase heterogeneous CO_2 catalysis. *Energy Environ. Sci.* **2019**, 12, 1122–1142.
(15) Sun, R.; Liao, Y.; Bai, S. T.; Zheng, M.; Zhou, C.; Zhang, T.; Sels, B. F. Heterogeneous catalysts for CO_2 hydrogenation to formic acid/formate: from nanoscale to single atom. *Energy Environ. Sci.* **2021**, 14, 1247–1285.
(16) Taghvaei, H.; Heravi, M.; Rahimpour, M. R. Synthesis of supported nanocatalysts via novel non-thermal plasma methods and its application in catalytic processes. *Plasma Process. Polym.* **2017**, 14, 1600204.
(17) Jia, L. Y.; Farouha, A.; Pinard, L.; Hedan, S.; Comparot, J. D.; Dufour, A.; Ben Tayeb, K.; Batiot-Dupeyrat, C. New routes for complete regeneration of coked zeolite. *Appl. Catal. B: Environ.* **2017**, 219, 82–91.
(18) Liu, S.; Winter, L. R.; Chen, J. G. Review of plasma-assisted catalysis for selective generation of oxygenates from CO_2 and CH_4. *ACS Catal.* **2020**, 10, 2855–2871.
(19) Li, S.; Dang, X.; Yu, X.; Abbas, G.; Zhang, Q.; Cao, L. The application of dielectric barrier discharge non-thermal plasma in VOCs abatement: a review. *Chem. Eng. J.* **2020**, 388, 124275.
(20) Liu, L.; Zhang, Z.; Das, S.; Kawi, S. Reforming of tar from biomass gasification in a hybrid catalysis-plasma system: a review. *Appl. Catal. B: Environ.* **2019**, 250, 250–272.
(21) Zhang, S.; Oehrlein, G. S. From thermal catalysis to plasma catalysis: a review of surface processes and their characterizations. *J. Phys. D: Appl. Phys.* **2021**, 213001.
(22) George, A.; Shen, B.; Craven, M.; Wang, Y.; Kang, D.; Wu, C.; Tu, X. A review of non-thermal plasma technology: a novel solution for CO_2 conversion and utilization. *Renew. Sust. Energy Rev.* **2021**, 135, 109702.
(23) Van Gessel, B.; Brandenburg, R.; Bruggeman, P. Electron properties and air mixing in radio frequency driven argon plasma jets at atmospheric pressure. *Appl. Phys. Lett.* **2013**, 103, 064103.
(24) Wang, Z.; Zhang, Y.; Neyts, E. C.; Cao, X.; Zhang, X.; Jang, B. W. L.; Liu, C. J. Catalyst preparation with plasmas: how does it work? *ACS Catal.* **2018**, 8, 2093–2110.
(25) Xu, J.; Zhang, Q.; Guo, F.; Xia, Y.; Tian, H. Coke resistance of Ni-based catalysts enhanced by cold plasma treatment for CH_4-CO_2 reforming: review. *Inter. J. Hydrogen Energy* **2021**, 46, 23174–23189.
(26) Di, L.; Zhang, J.; Zhang, X. A review on the recent progress, challenges, and perspectives of atmospheric-pressure cold plasma for preparation of supported metal catalysts. *Plasma Process Polym.* **2018**, 15, e1700234.
(27) Kim, S. H.; Moon, S. Y.; Park, J. Y. Non-colloidal nanocatalysts fabricated using arc plasma deposition and their applications in heterogeneous catalysis and photocatalysis. *Top. Catal.* **2017**, 60, 812–822.
(28) Chen, G.; Snyders, R.; Britun, N. CO_2 conversion using catalyst-free and catalyst-assisted plasma-processes: recent progress and understanding. *J. CO_2 Util.* **2021**, 49, 101557.
(29) Snoeckx, R.; Bogaerts, A. Plasma technology-a novel solution for CO_2 conversion? *Chem. Soc. Rev.* **2017**, 46, 5805–5863.
(30) Chen, G.; Godfroid, T.; Britun, N.; Georgieva, V.; Delplancke-Ogletree, M. P.; Snyders, R. Plasma-catalytic conversion of CO_2 and CO_2/H_2O in a surface-wave sustained microwave discharge. *Appl. Catal. B: Environ.* **2017**, 214, 114–125.
(31) Bian, L.; Zhang, L.; Xia, R.; Li, Z. Enhanced low-temperature CO_2 methanation activity on plasma-prepared Ni-based catalyst. *J Nat. Gas Sci. Eng.* **2015**, 27, 1189–1194.
(32) Guo, F.; Xu, J. Q.; Chu, W. CO_2 reforming of methane over Mn promoted Ni/Al_2O_3 catalyst treated by N_2 glow discharge plasma. *Catal. Today* **2015**, 256, 124–129.
(33) Liu, J.; Ma, Q.; Huang, Z.; Liu, G.; Zhang, H. Recent progress in graphene-based noble-metal nanocomposites for electrocatalytic applications. *Adv. Mater.* **2019**, 31, 1800696.
(34) Zhong, J.; Yang, X.; Wu, Z.; Liang, B.; Huang, Y.; Zhang, T. State of the art and perspectives in heterogeneous catalysis of CO_2 hydrogenation to methanol. *Chem. Soc. Rev.* **2020**, 49, 1385–1413.
(35) Zada, A.; Muhammad, P.; Ahmad, W.; Hussain, Z.; Ali, S.; Khan, M.; Khan, Q.; Maqbool, M. Surface plasmonic-assisted photocatalysis and optoelectronic devices with noble metal nanocrystals: design, synthesis and applications. *Adv. Funct. Mater.* **2020**, 30, 1906744.
(36) Akhundi, A.; Habibi-Yangjeh, A.; Abitorabi M.; Pouran, S. R. Review on photocatalytic conversion of carbon dioxide to value-added compounds and renewable fuels by graphitic carbon nitride-based photocatalysts. *Catal. Rev.* **2019**, 61, 595–628.
(37) Price, C. A. H.; Reina, T. R.; Liu, J. Engineering heterogenous catalysts for chemical CO_2 utilization: lessons from thermal catalysis and advantages of yolk@shell structured nanoreactors. *J. Energy Chem.* **2021**, 57, 304–324.
(38) Zhang, H.; Cheng, W.; Luan, D.; Lou, X. W. Atomically dispersed reactive centers for electrocatalytic CO_2 reduction and water splitting. *Angew. Chem. Int. Ed.* **2021**, 60, 13177–13196.
(39) Zou, J. J.; Zhang, Y. P.; Liu, C. J. Reduction of supported noble-metals ions using glow discharge plasma. *Langmuir* **2006**, 22, 11388–11394.
(40) Yan, J.; Pan, Y.; Cheetham, A. G.; Lin, Y. A.; Wang, W.; Cui, H.; Liu, C. J. One-step fabrication of self-assembled peptide thin films with highly dispersed noble metal nanoparticles. *Langmuir* **2013**, 29, 16051–16057.
(41) Zhao, Y.; Pan, Y. X.; Xie, Y.; Liu, C. J. Carbon dioxide reforming of methane over glow discharge plasma-reduced Ir/Al_2O_3 catalyst. *Catal. Commun.* **2008**, 9, 1558–1562.
(42) Rui, N.; Wang, Z.; Sun, K.; Ye, J.; Ge, Q.; Liu, C. J. CO_2 hydrogenation to methanol over Pd/In_2O_3: effects of Pd and oxygen vacancy. *Appl. Catal. B: Environ.* **2017**, 218, 488–497.
(43) Men, Y. L.; Liu, Y.; Wang, Q.; Luo, Z. H.; Shao, S.; Li, Y. B.; Pan, Y. X.

DOI: 10.14102/j.cnki.0254-5861.2022-0024

Highly dispersed Pt-based catalysts for selective CO_2 hydrogenation to methanol at atmospheric pressure. *Chem. Eng. Sci.* **2019**, 200, 167–175.
(44) Li, J.; Zhou, Y.; Tang, W.; Zheng, J.; Gao, X.; Wang, N.; Chen, X.; Wei, M.; Xiao, X.; Chu, W. Cold-plasma technique enabled supported Pt single atoms with tunable coordination for hydrogen evolution reaction. *Appl. Catal. B: Environ.* **2021**, 285, 119861.
(45) Shi, L.; Zhou, Y.; Tan, X.; Qi, S.; Smith, K. J.; Yi, C.; Yang, B.; Liu, S. Dielectric barrier discharge plasma grafting carboxylate groups on Pt/Al_2O_3 catalysts for highly efficient hydrogen release from perhydrodibenzyltoluene. *Catal. Sci. Technol.* **2022**, DOI: 10.1039/d1cy01652k.
(46) Men, Y. L.; Liu, P.; Peng, X.; Pan, Y. X. Efficient photocatalytic triggered by thin carbon layers coating on photocatalysis: recent progress and future perspective. *Sci. China Chem.* **2020**, 63, 1416–1427.
(47) Chen, S.; Chen, A. Electrochemical reduction of carbon dioxide on Au nanoparticles: an in situ FTIR study. *J. Phys. Chem. C* **2019**, 123, 23898–23906.
(48) Zhang, T.; Shang, H.; Zhang, B.; Yan, D.; Xiang, X. Ag/ultrathin-layered double hydroxide nanosheets induced by a self-redox strategy for highly selective CO_2 reduction. *ACS Appl. Mater. Interfaces* **2021**, 13, 16536–16544.
(49) Garba, M. D.; Usman, M.; Khan, S.; Shehzad, F.; Galadima, A.; Ehsan, M. F.; Ghanem, A. S.; Humayun, M. CO_2 towards fuels: a review of catalytic conversion of carbon dioxide to hydrocarbons. *J. Environ. Chem. Eng.* **2021**, 9, 104756.
(50) Franco, F.; Rettenmaier, C.; Jeon, H. S.; Cuenya, B. R. Transition metal-based catalysts for the electrochemical CO_2 reduction: from atoms and molecules to nanostructured materials. *Chem. Soc. Rev.* **2020**, 49, 6884–6946.
(51) Ao, C.; Feng, B.; Qian, S.; Wang, L.; Zhao, W.; Zhai, Y.; Zhang, L. Theoretical study of transition metals supported on $g\text{-}C_3N_4$ as electrochemical catalysts for CO_2 reduction to CH_3OH and CH_4. *J. CO_2 Util.* **2020**, 36, 116–123.
(52) Wang, D.; Xie, Z.; Porosoff, M. D.; Chen, J. G. Recent advances in carbon dioxide hydrogenation to produce olefins and aromatics. *Chem* **2021**, 7, 2277–2311.
(53) Dou, S.; Wang, X.; Wang, S. Rational design of transition metal-based materials for highly efficient electrocatalysis. *Small Methods* **2019**, 3, 1800211.
(54) Podrojková, N.; Sans, V.; Oriňak, A.; Oriňaková, R. Recent developments in the modeling of heterogeneous catalysts for CO_2 conversion to chemicals. *ChemCatChem* **2020**, 12, 1802–1825.
(55) Liu, C. J.; Ye, J.; Jiang, J.; Pan, Y. Progresses in the preparation of coke resistant Ni-based catalyst for steam and CO_2 reforming of methane. *ChemCatChem* **2011**, 3, 529–541.
(56) Fu, Z.; Wang, J.; Zhang, N.; Hao, K.; Yang, Z. Effects of substrate defects on the carbon cluster formation in graphene growth on Ni(111) surface. *Phys. Lett. A* **2014**, 378, 3055–3059.
(57) Liu, P.; Peng, X.; Men, Y. L.; Pan, Y. X. Recent progresses on improving CO_2 adsorption and proton production for enhancing efficiency of photocatalytic CO_2 reduction by H_2O. *Green Chem. Eng.* **2020**, 1, 33-39.
(58) Zhu, X.; Huo, P.; Zhang, Y. P.; Cheng, D. G.; Liu, C. J. Structure and reactivity of plasma treated Ni/Al_2O_3 catalyst for CO_2 reforming of methane. *Appl. Catal. B: Environ.* **2008**, 81, 132–140.
(59) Marinho, A. L. A.; Toniolo, F. S.; Noronha, F. B.; Epron, F.; Duprez, D.; Bion, N. Highly active and stable Ni dispersed on mesoporous $CeO_2\text{-}Al_2O_3$ catalysts for production of syngas by dry reforming of methane. *Appl. Catal. B: Environ.* **2021**, 281, 119459.
(60) Zou, J. J.; Liu, C. J.; Zhang, Y. P. Control of the metal-support interface of NiO-loaded photocatalysts via cold plasma treatment. *Langmuir* **2006**, 22, 2334–2339.
(61) Pan, Y. X.; Liu, C. J.; Shi, P. Preparation and characterization of coke resistant Ni/SiO_2 catalyst for carbon dioxide reforming of methane. *J. Power Sources* **2008**, 176, 46–53.
(62) Yan, X.; Hu, T.; Liu, P.; Li, S.; Zhao, B.; Zhang, Q.; Jiao, W.; Chen, S.; Wang, P.; Lu, J.; Fan, L.; Deng, X.; Pan, Y. X. Highly efficient and stable $Ni/CeO_2\text{-}SiO_2$ catalyst for dry reforming of methane: effect of interfacial structure of Ni/CeO_2 on SiO_2. *Appl. Catal. B: Environ.* **2019**, 246, 221–231.
(63) Jia, X.; Zhang, X.; Rui, N.; Hu, X.; Liu, C. J. Structural effect of Ni/ZrO_2 catalyst on CO_2 methanation with enhanced activity. *Appl. Catal. B: Environ.* **2019**, 244, 159–169.
(64) Rui, N.; Zhang, X.; Zhang, F.; Liu, Z.; Cao, X.; Xie, Z.; Zou, R.; Senanayake, S. D.; Yang, Y.; Rodriguez, J. A.; Liu, C. J. Highly active Ni/CeO_2 catalyst for CO_2 methanation: preparation and characterization. *Appl. Catal. B: Environ.* **2021**, 282, 119581.
(65) Zheng, X.; Wang, H.; Wen, J.; Peng, H. In_2S_3-NiS co-decorated $MoO_3@MoS_2$ composites for enhancing the solar-light induced CO_2 photoreduction activity. *Int. J. Hydrogen Energy* **2021**, 46, 36848–36858.
(66) Xu, J.; Xia, P.; Zhang, Q.; Guo, F.; Xia, Y.; Tian, H. Coke resistance of Ni-based catalysts enhanced by cold plasma treatment for $CH_4\text{-}CO_2$ reforming: review. *Int. J. Hydrogen Energy* **2021**, 46, 23174–23189.
(67) Sivachandiran, L.; Costa, P. D.; Khacef, A. CO_2 reforming in CH_4 over $Ni/g\text{-}Al_2O_3$ nano catalysts: effect of cold plasma surface discharge. *Appl. Surf. Sci.* **2020**, 501, 144175.
(68) Zhao, B.; Liu, P.; Li, S.; Shi, H.; Jia, X.; Wang, Q.; Yang, F.; Song, Z.; Guo, C.; Hu, J.; Chen, Z.; Yan, X.; Ma, X. Bimetallic Ni-Co nanoparticles on SiO_2 as robust catalyst for CO methanation: effect of homogeneity of Ni-Co alloy. *Appl. Catal. B: Environ.* **2020**, 278, 119307.
(69) Ahmad, F.; Lovell, E. C.; Masood, H.; Cullen, P. J.; Ostrikov, K. K.; Scott, J. A.; Amal, R. Low-temperature CO_2 methanation: synergistic effects in plasma-Ni hybrid catalytic system. *ACS Sustainable Chem. Eng.* **2020**, 8, 1888–1898.
(70) Wang, B.; Xiong, Y.; Han, Y.; Hong, J.; Zhang, Y.; Li, J.; Jing, F.; Chu, W. Preparation of stable and highly active Ni/CeO_2 catalysts by glow discharge plasma technique for glycerol steam reforming. *Appl. Catal. B: Environ.* **2019**, 249, 257–265.
(71) Tang, W.; Li, J.; Zheng, J.; Chu, W.; Wang, N. Atomically dispersed metal sites stabilized on a nitrogen doped carbon carrier via N_2 glow- discharge plasma. *Chem. Commun.* **2020**, 56, 9198–9201.
(72) Ronda-Lloret, M.; Wang, Y.; Oulego, P.; Rothenberg, G.; Tu, X. CO_2 hydrogenation at atmospheric pressure and low temperature using plasma-enhanced catalysis over supported cobalt oxide catalysts. *ACS Sustainable Chem. Eng.* **2020**, 8, 17397–17407.

Received: February 5, 2022
Accepted: February 22, 2022
Published: April 8, 2022